Degenerate Chenciner bifurcation revisited

G. Moza,* O. Brandibur,† E.A. Kokovics, L.F. Vesa

Abstract

Generic results for degenerate Chenciner (generalized Neimark-Sacker) bifurcation are obtained in the present work. The bifurcation arises in two-dimensional discrete-time systems with two independent parameters. We define in this work a new transformation of parameters, which enables the study of the bifurcation when the degeneracy occurs. By the four bifurcation diagrams we obtain, new behaviors hidden by the degeneracy are brought to light.

1 Introduction

Many real-world applications are modeled using dynamical systems described by both differential equations and their discrete-time counterparts, namely, difference equations. A discrete-time approach for studying various models is proved to be efficient, especially from a computational point of view. They may uncover complex behaviors which are not easily captured by a continuous-time approach. A review on continuous-time versus discrete-time approaches in scheduling of chemical processes is presented in [7]. The study of discrete-time dynamical systems is an active field of research [2], [6]–[10], [12]–[16]. The analysis of bifurcations is among the most relevant topics in the qualitative theory of dynamical systems, particularly, in discrete-time systems [17].

In this work, we focus our attention on the Chenciner bifurcation (known also as the generalized Neimark-Sacker bifurcation) [Chenciner, 1985, 1988], [5], which arises in two-dimensional discrete-time dynamical systems with two real parameters. The presence of this bifurcation in a three-mass chain model has been reported in [1]. The non-degenerate case of this bifurcation has been studied earlier [11], while a degenerate case has been recently presented in [15].

The purpose of this paper is to further study the degenerate case from [15], by considering a different approach, which reduces the number of bifurcation diagrams that are needed to describe the bifurcation in the degenerate case.

The paper is organized as it follows. After the introduction, in section two we present the main ingredients of the bifurcation and establish the research objectives to be explored later in the work. Section three presents briefly the general results which are needed for studying the bifurcation in a degenerate framework. The main results of the paper are comprised in section four, where we define a new transformation of parameters for the degeneracy we study. Using this change we obtain four bifurcation diagrams, which describe the behavior of the system when the degeneracy occurs. The last section contains conclusive remarks on our results.

*Department of Mathematics, Politehnica University of Timisoara, Romania; email: gheorghe.moza@upt.ro

†Department of Mathematics, West University of Timisoara, Romania

2 Preliminaries

Consider the discrete-time system

$$x_{n+1} = f(x_n, \alpha), \tag{1}$$

where $x_n \in \mathbb{R}^2$, $n \in \mathbb{Z}$, $\alpha = (\alpha_1, \alpha_2) \in \mathbb{R}^2$ and f is a smooth function of class C^r with $r \geq 2$. Another form of (1) which avoids indices is

$$x \longmapsto f(x, \alpha). \tag{2}$$

Using complex coordinates, (2) can be written as

$$z \longmapsto \delta(\alpha) z + g(z, \bar{z}, \alpha), \tag{3}$$

where δ and g are smooth functions, $\delta(\alpha) = r(\alpha) e^{i\theta(\alpha)}$ and $g(z, \bar{z}, \alpha) = \sum_{k+l \geq 2} \frac{1}{k!l!} g_{kl}(\alpha) z^k \bar{z}^l$, with $r(0) = 1$ and $\theta(0) = \theta_0$; $g_{kl}(\alpha)$ are smooth complex-valued functions.

Equation (3) can be further transformed as in [11] to

$$w \longmapsto \left(r(\alpha) + b_1(\alpha) w\bar{w} + b_2(\alpha) w^2 \bar{w}^2 \right) w e^{i\theta(\alpha)} + O\left(|w|^6 \right), \tag{4}$$

where $b_k(\alpha) = a_k(\alpha) e^{-i\theta(\alpha)}$, $k = 1, 2$.

Remark 2.1. *Equation (3) becames (4) by using the following invertible smoothly parameter change of complex coordinate*

$$z = w + \sum_{2 \leq k+l \leq 5} \frac{1}{k!l!} h_{kl}(\alpha) w^k \bar{w}^l, \quad h_{21}(\alpha) = h_{32}(\alpha) = 0.$$

Denoting by

$$\beta_1(\alpha) = r(\alpha) - 1 \text{ and } \beta_2(\alpha) = Re\left(b_1(\alpha) \right), \tag{5}$$

and using polar coordinates, (4) becomes

$$\begin{cases} \rho_{n+1} = & \rho_n \left(1 + \beta_1(\alpha) + \beta_2(\alpha) \rho_n^2 + L_2(\alpha) \rho_n^4 \right) + \rho_n O\left(\rho_n^6 \right) \\ \varphi_{n+1} = & \varphi_n + \theta(\alpha) + \rho_n^2 \left(\frac{Im(b_1(\alpha))}{\beta_1(\alpha)+1} + O\left(\rho_n, \alpha \right) \right) \end{cases}, \tag{6}$$

where $L_2(\alpha) = \frac{Im^2(b_1(\alpha)) + 2(1+\beta_1(\alpha)) Re(b_2(\alpha))}{2(\beta_1(\alpha)+1)}$.

A bifurcation in the system (6) satisfying $r(0) = 1$, $Re(b_1(0)) = 0$ and $L_2(0) \neq 0$, is known as the *Chenciner bifurcation*. Since $\beta_1(0) = 0$, it follows that

$$L_2(0) = \frac{1}{2} \left(Im^2(b_1(0)) + 2Re(b_2(0)) \right).$$

When the transformation of parameters

$$(\alpha_1, \alpha_2) \longmapsto (\beta_1(\alpha), \beta_2(\alpha)) \tag{7}$$

is regular at $(0, 0)$, then β_1 and β_2 become the new parameters of the system (6). This is the *non-degenerate case* of the bifurcation.

The aim of this paper is to study the bifurcation in the *degenerate* case with respect to the transformation of parameters (7), namely, when (7) is not regular at $(0, 0)$. Hence, we cannot use $\beta_{1,2}$ as new parameters of the system (6), due to this degeneracy condition. Alternatively, we could keep on working with the initial parameters $\alpha_{1,2}$ in the polar form (6), as it is done in [15], or explore for another regular transformation of the parameters. We opt for the second method in this paper.

3 Analysis of degenerate Chenciner bifurcation

The truncated form of the $\rho-$map of (6) obtained by eliminating higher order terms is

$$\rho_{n+1} = \rho_n \left(1 + \beta_1(\alpha) + \beta_2(\alpha)\rho_n^2 + L_2(\alpha)\rho_n^4\right). \tag{8}$$

The $\varphi-$map of (6), which describes a rotation by an angle depending on α and ρ, can be approximated by its truncated form

$$\varphi_{n+1} = \varphi_n + \theta(\alpha). \tag{9}$$

Assume $0 < \theta(0) < \pi$. Henceforward, the system to be studied in this paper is (8)-(9), which is known as *the (truncated) normal form* of the system (4). The main equation shaping the dynamics of the system (8)-(9) is the $\rho-$map (8), which is independent from the $\varphi-$map and therefore, will be studied separately.

Defining a one-dimensional dynamical system, the $\rho-$map has the fixed point $\rho = 0$, for all values of α, which corresponds to the fixed point $O(0,0)$ in the normal form (8)-(9). A positive nonzero fixed point of the $\rho-$map corresponds to an invariant closed curve in (8)-(9).

Observe that $sign(L_2(\alpha)) = sign(L_0)$ for $|\alpha| = \sqrt{\alpha_1^2 + \alpha_2^2}$ sufficiently small, as

$$L_2(\alpha) = L_0(1 + O(|\alpha|)) \quad \text{and} \quad L_0 \neq 0.$$

Throughout the work, $O(|\alpha|^n)$ denotes the higher order terms in a Taylor expansion at $\alpha = 0$. For example,

$$O(|\alpha|) = k_{10}\alpha_1 + k_{01}\alpha_2 + ... \quad \text{and} \quad O\left(|\alpha|^2\right) = k_{20}\alpha_1^2 + k_{11}\alpha_1\alpha_2 + k_{02}\alpha_2^2 + ...$$

The next Proposition 3.1 describes the stability of O for $|\alpha|$ sufficiently small, while Theorem 3.2 deals with the existence of invariant closed curves in the normal form (8)-(9). Their proofs can be obtained by studying (8) and are presented in [15].

Proposition 3.1. *The fixed point O is (linearly) stable if $\beta_1(\alpha) < 0$ and unstable if $\beta_1(\alpha) > 0$, for all values α with $|\alpha|$ sufficiently small. On the bifurcation curve $\beta_1(\alpha) = 0$, O is (nonlinearly) stable if $\beta_2(\alpha) < 0$ and unstable if $\beta_2(\alpha) > 0$, when $|\alpha|$ is sufficiently small. At $\alpha = 0$, O is (nonlinearly) stable if $L_0 < 0$ and unstable if $L_0 > 0$.*

The positive nonzero fixed points of the $\rho-$map (8), which are the solutions of the equation

$$L_2(\alpha)y^2 + \beta_2(\alpha)y + \beta_1(\alpha) = 0, \tag{10}$$

where $y = \rho_n^2$, generate invariant closed curves (invariant circles) in the system (8)-(9).

Denote by

$$\Delta(\alpha) = \beta_2^2(\alpha) - 4\beta_1(\alpha)L_2(\alpha), \tag{11}$$

respectively, $y_1 = \frac{1}{2L_2(\alpha)}\left(\sqrt{\Delta(\alpha)} - \beta_2(\alpha)\right)$ and $y_2 = -\frac{1}{2L_2(\alpha)}\left(\sqrt{\Delta(\alpha)} + \beta_2(\alpha)\right)$ the two roots of (10), whenever they exist as real numbers.

Theorem 3.2. *The following assertions are true.*
1) When $\Delta(\alpha) < 0$ for all $|\alpha|$ sufficiently small, the normal form (8)-(9) has no invariant circles.
2) When $\Delta(\alpha) > 0$ for all $|\alpha|$ sufficiently small, the normal form (8)-(9) has:
*   a) one invariant unstable circle $\rho_n = \sqrt{y_1}$ if $L_0 > 0$ and $\beta_1(\alpha) < 0$;*

3

b) one invariant stable circle $\rho_n = \sqrt{y_2}$ if $L_0 < 0$ and $\beta_1(\alpha) > 0$;

c) two invariant circles, $\rho_n = \sqrt{y_1}$ unstable and $\rho_n = \sqrt{y_2}$ stable, if $L_0 > 0$, $\beta_1(\alpha) > 0$, $\beta_2(\alpha) < 0$ or $L_0 < 0$, $\beta_1(\alpha) < 0$, $\beta_2(\alpha) > 0$; in addition, $y_1 < y_2$ if $L_0 < 0$ and $y_2 < y_1$ if $L_0 > 0$;

d) no invariant circles if $L_0 > 0$, $\beta_1(\alpha) > 0$, $\beta_2(\alpha) > 0$ or $L_0 < 0$, $\beta_1(\alpha) < 0$, $\beta_2(\alpha) < 0$.

3) On the bifurcation curve $\Delta(\alpha) = 0$, the system (8)-(9) has one invariant unstable circle $\rho_n = \sqrt{y_1}$ for all $L_0 \neq 0$.

4) When $\beta_1(\alpha) = 0$, the system (8)-(9) has one invariant circle $\rho_n = \sqrt{-\frac{\beta_2(\alpha)}{L_0}}$ whenever $L_0 \beta_2(\alpha) < 0$. It is stable if $L_0 < 0$ and $\beta_2(\alpha) > 0$, respectively, unstable if $L_0 > 0$ and $\beta_2(\alpha) < 0$.

4 Bifurcation diagrams

The transformation (7) is not regular at $\alpha = 0$ and, thus, the Chenciner bifurcation is *degenerate*, if and only if $\left. \frac{\partial \beta_1}{\partial \alpha_1} \frac{\partial \beta_2}{\partial \alpha_2} - \frac{\partial \beta_1}{\partial \alpha_2} \frac{\partial \beta_2}{\partial \alpha_1} \right|_{\alpha=0} = 0$. Denoting the coefficients of the linear parts of $\beta_{1,2}(\alpha)$ by $\frac{\partial \beta_1}{\partial \alpha_i}(0) = c_i$, respectively, $\frac{\partial \beta_2}{\partial \alpha_i}(0) = d_i$, $i = 1, 2$, the degeneracy condition becomes

$$c_1 d_2 - c_2 d_1 = 0. \tag{12}$$

Assume $c_i \neq 0$ and $d_i \neq 0$. Denote by $L_2(\alpha) = L_0 + l_1 \alpha_1 + l_2 \alpha_2 + O\left(|\alpha|^2\right)$. In general, denote by $\beta_1(\alpha) = c_1 \alpha_1 + c_2 \alpha_2 + \sum\limits_{i+j=2}^{m} c_{ij} \alpha_1^i \alpha_2^j + O\left(|\alpha|^{m+1}\right)$ and $\beta_2(\alpha) = d_1 \alpha_1 + d_2 \alpha_2 + \sum\limits_{i+j=2}^{n} d_{ij} \alpha_1^i \alpha_2^j + O\left(|\alpha|^{n+1}\right)$.

Theorem 4.1. *Assume the degeneracy condition (12) holds true. Then, there exists a transformation of parameters $(\alpha_1, \alpha_2) \overset{S}{\longmapsto} (\mu_1, \mu_2)$ given by*

$$\mu_1 = \beta_2^2(\alpha) - 4\beta_1(\alpha) L_2(\alpha) \ \ and \ \mu_2 = \beta_2(\alpha) + L_2(\alpha) - L_0, \tag{13}$$

which is regular at $\alpha = 0$ iff

$$c_1 l_2 - c_2 l_1 \neq 0. \tag{14}$$

Denote by $\widehat{\beta}_{1,2}(\mu) = \beta_{1,2} \circ S^{-1}(\mu)$. In the new parametric plane $\mu_1 \mu_2$ and for $|\mu|$ sufficiently small, $\widehat{\beta}_1(\mu) = 0$ is a curve of the form

$$B_1 = \left\{ (\mu_1, \mu_2) \in \mathbb{R}^2, \mu_1 = m_2^2 \mu_2^4 (1 + O(\mu_2)) \right\}, \tag{15}$$

while $\widehat{\beta}_2(\mu) = 0$ a curve given by

$$B_2 = \left\{ (\mu_1, \mu_2) \in \mathbb{R}^2, \mu_1 = 4L_0 \frac{c_1}{d_1} m_2 \mu_2^2 (1 + O(\mu_2)) \right\}, \tag{16}$$

where m_2 is a real constant depending on the linear and quadratic coefficients of $\beta_{1,2}(\alpha)$ and $L_2(\alpha)$.

Proof. For the transformation S, denote by $A(\alpha) = \begin{pmatrix} \frac{\partial \mu_1}{\partial \alpha_1}(\alpha) & \frac{\partial \mu_1}{\partial \alpha_2}(\alpha) \\ \frac{\partial \mu_2}{\partial \alpha_1}(\alpha) & \frac{\partial \mu_2}{\partial \alpha_2}(\alpha) \end{pmatrix}$. Using the linear terms of $\beta_{1,2}(\alpha)$ and $L_2(\alpha)$, the matrix $A(\alpha)$ at $\alpha = 0$ becomes $A_0 = \begin{pmatrix} -4L_0 c_1 & -4L_0 c_2 \\ d_1 + l_1 & d_2 + l_2 \end{pmatrix}$.

4

The inverse transformation $(\mu_1, \mu_2) \overset{S^{-1}}{\longmapsto} (\alpha_1, \alpha_2)$ in its linear terms can be determined from $(\mu_1, \mu_2)^T = A_0 \cdot (\alpha_1, \alpha_2)^T$, that is, $(\alpha_1, \alpha_2)^T = A_0^{-1} (\mu_1, \mu_2)^T$. We obtain

$$\alpha_1 = s_{10}\mu_1 + s_{01}\mu_2 \text{ and } \alpha_2 = p_{10}\mu_1 + p_{01}\mu_2, \tag{17}$$

where $s_{10} = -\frac{d_2+l_2}{4L_0 n_0}$, $s_{01} = -\frac{c_2}{n_0}$, $p_{10} = \frac{d_1+l_1}{4L_0 n_0}$, $p_{01} = \frac{c_1}{n_0}$, and $n_0 = c_1 d_2 - c_2 d_1 + c_1 l_2 - c_2 l_1$.

The inverse transformation S^{-1} can be determined in further order terms. For example, S^{-1} in quadratic terms is of the form

$$\alpha_1 = \sum_{i+j=1}^{2} s_{ij}\mu_1^i \mu_2^j \text{ and } \alpha_2 = \sum_{i+j=1}^{2} p_{ij}\mu_1^i \mu_2^j. \tag{18}$$

The coefficients s_{ij} and p_{ij} can be determined in terms of the coefficients of $\beta_{1,2}(\alpha)$ and $L_2(\alpha)$ by the method of undetermined coefficients in (13).

It follows from (12) that

$$\det(A_0) = -4L_0 (c_1 l_2 - c_2 l_1),$$

thus, since $L_0 \neq 0$, the new transformation S is regular at $\alpha = 0$ if and only if $c_1 l_2 - c_2 l_1 \neq 0$.

Using (12) in (17), $L_2(\alpha) = L_0 + l_1 \alpha_1 + l_2 \alpha_2 + O\left(|\alpha|^2\right)$ becomes $\widehat{L}_2(\mu) = L_2 \circ S^{-1}(\mu)$ given by

$$\widehat{L}_2(\mu) = L_0 + \frac{d_1}{4L_0 c_1}\mu_1 + \mu_2 + O\left(|\mu|^2\right), \tag{19}$$

respectively, $\widehat{\beta}_2(\mu) = \beta_2 \circ S^{-1}(\mu)$ by (13) reads

$$\widehat{\beta}_2(\mu) = \mu_2 - \widehat{L}_2(\mu) + L_0 = -\frac{1}{4}\frac{d_1}{L_0 c_1}\mu_1 + O\left(|\mu|^2\right).$$

In order to determine $\widehat{\beta}_2(\mu)$ in its lowest terms, write $\widehat{L}_2(\mu)$ from (19) in the form

$$\widehat{L}_2(\mu) = L_0 + \frac{d_1}{4L_0 c_1}\mu_1 (1 + O(|\mu|)) + \mu_2 - m_2 \mu_2^2 (1 + O(\mu_2)),$$

where m_2 is assumed nonzero, $m_2 \neq 0$. Then,

$$\widehat{\beta}_2(\mu) = -\frac{d_1}{4L_0 c_1}\mu_1 (1 + O(|\mu|)) + m_2 \mu_2^2 (1 + O(\mu_2)). \tag{20}$$

Since $\widehat{\beta}_2(0,0) = 0$ and $\frac{\partial \widehat{\beta}_2}{\partial \mu_1}(0,0) = -\frac{1}{4}\frac{d_1}{L_0 c_1} \neq 0$, we can apply the Implicit Function Theorem to the equation $\widehat{\beta}_2(\mu_1, \mu_2) = 0$ given by (20). Thus, there exists $\varepsilon > 0$ sufficiently small and a function

$$\mu_1 : (-\varepsilon, \varepsilon) \to \mathbb{R}, \ \mu_1 = \mu_1(\mu_2),$$

such that $\mu_1(0) = 0$ and $\widehat{\beta}_2(\mu_1(\mu_2), \mu_2) = 0$ for all $|\mu_2| < \varepsilon$; μ_1 becomes a function of argument μ_2 in (20), $\mu_1 = \mu_1(\mu_2)$. Deriving now in $-\frac{d_1}{4L_0 c_1}\mu_1(1 + O(|\mu|)) + m_2\mu_2^2(1 + O(\mu_2)) = 0$ with respect to μ_2, where $\mu_1 = \mu_1(\mu_2)$, we obtain $\frac{\partial \mu_1}{\partial \mu_2}(0) = 0$ and $\frac{\partial^2 \mu_1}{\partial \mu_2^2}(0) = 8L_0 \frac{c_1}{d_1}m_2$.

Expressing $\mu_1 = \mu_1(0) + \frac{\partial \mu_1}{\partial \mu_2}(0)\mu_2 + \frac{1}{2}\frac{\partial^2 \mu_1}{\partial \mu_2^2}(0)\mu_2^2 + O\left(\mu_2^3\right)$ as a Taylor series at $\mu_2 = 0$, we obtain

$$\mu_1 = 4L_0 \frac{c_1}{d_1}m_2 \mu_2^2 (1 + O(\mu_2)). \tag{21}$$

5

Similarly, by (12), (17), (13) and (20), $\widehat{\beta}_1(\mu) = -\frac{1}{4\widehat{L}_2(\mu)}\left(\mu_1 - \widehat{\beta}_2^2(\mu)\right)$ becomes

$$\widehat{\beta}_1(\mu) = -\frac{1}{4L_0}\left[\mu_1\left(1 + O(|\mu|)\right) - m_2^2\mu_2^4\left(1 + O(\mu_2)\right)\right], \tag{22}$$

which, by the Implicit Function Theorem, leads to B_1.

The exact expression of m_2 is not essential in the qualitative analysis of the Chenciner bifurcation we aim to obtain in this article. However, since in concrete applications it is useful, we determine it. To this end, using (18) in $L_2(\alpha) = L_0 + l_1\alpha_1 + l_2\alpha_2 + l_{20}\alpha_1^2 + l_{11}\alpha_1\alpha_2 + l_{02}\alpha_2^2$, it follows that the term $-m_2\mu_2^2$ of $\widehat{L}_2(\mu)$ has the coefficient $m_2 = -\left(l_{02}p_{01}^2 + l_{11}p_{01}s_{01} + l_{20}s_{01}^2 + l_2p_{02} + l_1s_{02}\right)$.

We need further the inverse transformation (18), more exactly, we need the coefficients s_{ij} and p_{ij} with $i + j = 1$ (which are already known), respectively, s_{02} and p_{02}. Substituting for α_1 and α_2 from (18) in the transformation (13) and using the method of undetermined coefficients, we find

$$p_{02} = d_1\frac{d_1^3c_{02} - d_1^2(c_1d_{02} + c_1l_{02} - l_1c_{02}) - d_2^2(c_1d_{20} + c_1l_{20} - l_1c_{20}) + d_1d_2(c_1d_{11} - d_1c_{11} + d_2c_{20} + c_1l_{11} - l_1c_{11})}{c_1(d_1l_2 - d_2l_1)^3}$$

and

$$s_{02} = \frac{-(d_2c_{02} + l_2c_{02})d_1^3 + (c_1d_{02} + d_2c_{11} + c_1l_{02} + l_2c_{11})d_1^2d_2 - (c_1d_{11} + d_2c_{20} + c_1l_{11} + l_2c_{20})d_1d_2^2 + c_1d_2^3(d_{20} + l_{20})}{c_1(d_1l_2 - d_2l_1)^3}.$$

These yield

$$m_2 = -\frac{c_{02}d_1^3 - c_{11}d_1^2d_2 - c_1d_{02}d_1^2 + c_{20}d_1d_2^2 + c_1d_{11}d_1d_2 - c_1d_{20}d_2^2}{c_1\left(d_1l_2 - d_2l_1\right)^2}. \tag{23}$$

Notice that, the both curves $\widehat{\beta}_{1,2}(\mu) = 0$ are tangent to the μ_2−axis at the origin and they are parabola-like curves. $\square$

Remark 4.2. *The new non-degeneracy condition (14) does not use any coefficient from $\beta_2(\alpha)$ but only from $\beta_1(\alpha)$ and $L(\alpha)$.*

The equation (10) becomes

$$\widehat{L}_2(\mu)y^2 + \widehat{\beta}_2(\mu)y + \widehat{\beta}_1(\mu) = 0, \tag{24}$$

where $\widehat{L}_2(\mu) = L_0(1 + O(|\mu|)) \neq 0$. The new discriminant of (24) is $\widehat{\Delta}(\mu) = \Delta \circ S^{-1}(\mu)$, which, by the transformation (13), becomes

$$\widehat{\Delta}(\mu) = \mu_1, \tag{25}$$

while $\widehat{\beta}_{1,2}(\mu)$ are given in (22) and (20).

Remark 4.3. *The following theorem describes the bifurcation diagrams of the system (8)-(9) in the new parametric space $\mu_1O\mu_2$. In elaborating the diagrams from Figure 1 and Figure 2, the curves B_1 and B_2 are approximated by (B_1) $\mu_1 = m_2^2\mu_2^4$ and (B_2) $\mu_1 = 4L_0\frac{c_1}{d_1}m_2\mu_2^2$, which are parabola-like curves. Their relative positions one to another are given by m_2, L_0 and $\frac{c_1}{d_1}$. By (25), the curve $\widehat{\Delta}(\mu) = 0$ coincides to the μ_2−axes.*

Theorem 4.4. *The behavior of the system (8)-(9) is described by four bifurcation diagrams. More exactly, by Figure 1 if $L_0 < 0$, respectively, Figure 2 if $L_0 > 0$.*

Proof. Let $\left(\mu_1^{B_1}, \mu_2\right) \in B_1$ and $\left(\mu_1^{B_2}, \mu_2\right) \in B_2$ be two points from the two curves. Then, (15) and (16) yield

$$\mu_1^{B_2} - \mu_1^{B_1} = k_1 \mu_2^2 \left(1 + O\left(\mu_2\right)\right) \neq 0, \tag{26}$$

for $|\mu_2|$ sufficiently small, $\mu_2 \neq 0$, where $k_1 = 4L_0 \frac{c_1}{d_1} m_2$.

Notice that B_1 lies in $\{\mu_1 > 0\}$ for all $m_2 \neq 0$, while $B_2 \subset \{\mu_1 > 0\}$ if $k_1 > 0$, respectively, $B_2 \subset \{\mu_1 < 0\}$ if $k_1 < 0$.

Assume first $L_0 < 0$, $m_2 < 0$ and $c_1 d_1 < 0$, thus, $k_1 < 0$. Then $B_2 \subset \{\mu_1 < 0\}$ and $\widehat{\beta}_1(\mu) = -\frac{1}{4L_0}\left(\mu_1 - m_2^2 \mu_2^4\right) > 0$ inside the parabola B_1 (corresponding to $\mu_1 > 0$) and $\widehat{\beta}_1(\mu) < 0$ on the exterior of B_1, Figure 1. It follows from the Table 1 that, the phase portrait is 4 whenever $L_0 < 0$ and $\widehat{\beta}_1(\mu) < 0$, for any signs of $\widehat{\beta}_2(\mu)$ and $\widehat{\Delta}(\mu)$, including on $\widehat{\Delta}(\mu) = 0$. Notice that $\widehat{\beta}_2(\mu) = -\frac{d_1}{4L_0 c_1}\mu_1 + m_2 \mu_2^2 < 0$ on $\widehat{\Delta}(\mu) = \mu_1 > 0$. On the other hand, the phase portrait is 3 if $L_0 < 0$, $\widehat{\beta}_1(\mu) > 0$ and $\widehat{\Delta}(\mu) = \mu_1 > 0$, independent on the sign of $\widehat{\beta}_2(\mu)$, by Table 1. These prove the bifurcation diagram is D_1 from Figure 1.

Assume now $c_1 d_1 > 0$, while $L_0 < 0$ and $m_2 < 0$. Then $B_1, B_2 \subset \{\mu_1 > 0\}$ and, by (26), $\mu_1^{B_2} > \mu_1^{B_1} > 0$, thus, the parabola B_2 lies in the interior of the parabola B_1, where $\widehat{\beta}_1(\mu) > 0$ and $\widehat{\Delta}(\mu) = \mu_1 > 0$. Thus, by Table 1, the phase portrait is 3 in the interior of B_1 for any sign of $\widehat{\beta}_2(\mu)$, respectively, 4 in the exterior of B_1 because $\widehat{\beta}_2(\mu) = -\frac{d_1}{4L_0 c_1}\mu_1 + m_2 \mu_2^2 < 0$ on the exterior of B_1. Thus, the same bifurcation diagram D_1, Figure 1, characterizes the dynamics of the system (8)-(9) in this case.

In the second case, assume $L_0 < 0$ and $m_2 > 0$, and consider first $c_1 d_1 > 0$, thus, $k_1 < 0$. Then $B_2 \subset \{\mu_1 < 0\}$ and $\widehat{\beta}_1(\mu) > 0$ inside of B_1 ($\mu_1 > 0$) and $\widehat{\beta}_1(\mu) < 0$ on the exterior of B_1, Figure 1(D_2). By Table 1, the phase portrait is 4 whenever $L_0 < 0$, $\widehat{\Delta}(\mu) = \mu_1 < 0$ and $\widehat{\beta}_1(\mu) < 0$, for any signs of $\widehat{\beta}_2(\mu)$. On $\widehat{\Delta}(\mu) = 0$, the phase portrait becomes 5 since $\widehat{\beta}_2(\mu) > 0$ on $\mu_1 \geq 0$, while on the exterior of B_1 and $\mu_1 > 0$, it is 7 because $\widehat{\beta}_1(\mu) < 0$. On B_1 and the interior of B_1, it becomes 3, because $\widehat{\beta}_{1,2}(\mu) > 0$ and $\widehat{\Delta}(\mu) > 0$. Thus, the bifurcation diagram corresponding to this case is D_2 from Figure 1.

When $c_1 d_1 < 0$, $L_0 < 0$ and $m_2 > 0$, the curves $B_{1,2} \subset \{\mu_1 > 0\}$ with $k_1 > 0$. By (26), $\mu_1^{B_2} > \mu_1^{B_1} > 0$, thus, the parabola B_2 lies again in the interior of the parabola B_1, where $\widehat{\beta}_1(\mu) > 0$ and $\widehat{\Delta}(\mu) > 0$. It follows from Table 1 that, the phase portrait is 3 inside of B_1, independent on the sign of $\widehat{\beta}_2(\mu)$, while it remains 3 on B_1 because $\widehat{\beta}_2(\mu) > 0$ on the exterior of B_2. Further, on the exterior of B_1 and $\mu_1 > 0$, the phase portrait becomes 7, since $L_0 < 0$, $\widehat{\beta}_1(\mu) < 0$, $\widehat{\Delta}(\mu) > 0$ and $\widehat{\beta}_2(\mu) > 0$, which transforms in 5 on $\mu_1 = 0$, respectively, in 4 on $\mu_1 < 0$, because $L_0 < 0$, $\widehat{\beta}_1(\mu) < 0$, $\widehat{\Delta}(\mu) < 0$ and $\widehat{\beta}_2(\mu) > 0$. Therefore, the bifurcation diagram corresponding to this case is D_2 as well.

One can proceed similarly for the case $L_0 > 0$. Two bifurcation diagrams, D_3 and D_4 from Figure 2, describe the dynamics of the system (8)-(9) in this case. $\square$

The bifurcation regions we encounter in our study are among the ones given in Table 1, which were described in Theorem 4.4. Figure 3 illustrates the possible generic phase portraits corresponding to the regions from the two tables.

Figure 1: Bifurcation diagrams corresponding to $L_0 < 0$, $c_1 d_1 \neq 0$, respectively, $m_2 < 0$ and $m_2 > 0$.

Table 1. *The regions in the parametric plane $\mu_1 \mu_2$ defined by $\widehat{\Delta}(\mu)$, $\widehat{\beta}_{1,2}(\mu)$ and L_0.*

L_0	$\widehat{\Delta}(\mu)$	$\widehat{\beta}_1$	$\widehat{\beta}_2$	Region	L_0	$\widehat{\Delta}(\mu)$	$\widehat{\beta}_1$	$\widehat{\beta}_2$	Region
$-$	$-$	$-$	$\pm, 0$	4	$+$	$+$	$-$	$\pm, 0$	1
$-$	$+$	$-$	$-$	4	$+$	$+$	0	$-$	1
$-$	0	$-$	$-$	4	$+$	$-$	$+$	$\pm, 0$	2
$-$	$+$	0	$-$	4	$+$	$+$	$+$	$+$	2
$-$	0	0	0	4	$+$	0	$+$	$+$	2
$-$	$+$	$+$	$\pm, 0$	3	$+$	$+$	0	$+$	2
$-$	$+$	0	$+$	3	$+$	0	0	0	2
$-$	$+$	$-$	$+$	7	$+$	0	$+$	$-$	6
$-$	0	$-$	$+$	5	$+$	$+$	$+$	$-$	8

Example 4.5. *Consider a two-dimensional map $(\rho_n, \varphi_n) \longmapsto (\rho_{n+1}, \varphi_{n+1})$ given in polar coordinates by*

$$
\begin{cases}
\rho_{n+1} = & \rho_n \left(1 + \beta_1(\alpha) + \beta_2(\alpha) \rho_n^2 + L_2(\alpha) \rho_n^4 \right) \\[2mm]
\varphi_{n+1} = & \varphi_n + \theta_0
\end{cases}
, \qquad (27)
$$

where θ_0 is fixed, $0 < \theta_0 < \pi$, $\beta_1(\alpha) = \alpha_1 + \alpha_2 + 2\alpha_1^2 + \alpha_2^2$, $\beta_2(\alpha) = \alpha_1 + \alpha_2 + 2\alpha_1 \alpha_2$ and $L_2(\alpha) = 1 + \alpha_1 + 2\alpha_2 + \alpha_1^2 + \alpha_2^3$.

Remark 4.6. *The map (27) is degenerate with respect to the change of parameters $(\alpha_1, \alpha_2) \longmapsto (\beta_1, \beta_2)$ since $c_1 d_2 - c_2 d_1 = 0$, thus, it cannot be studied with the known methods for the non-degenerate case. On the other hand, the transformation (13) proposed in this paper, $(\alpha_1, \alpha_2) \xrightarrow{S} (\mu_1, \mu_2)$, is regular at $(0,0)$ since (14) is satisfied, thus, it can be applied to study the degenerate Chenciner bifurcation in this map.*

The inverse transformation S^{-1} in its linear terms is given by $\alpha_1 = -\frac{3}{4}\mu_1 - \mu_2$ and $\alpha_2 = \frac{1}{2}\mu_1 + \mu_2$. In order to find m_2 without applying (23), we need S^{-1} in its linear and quadratic terms, which is of
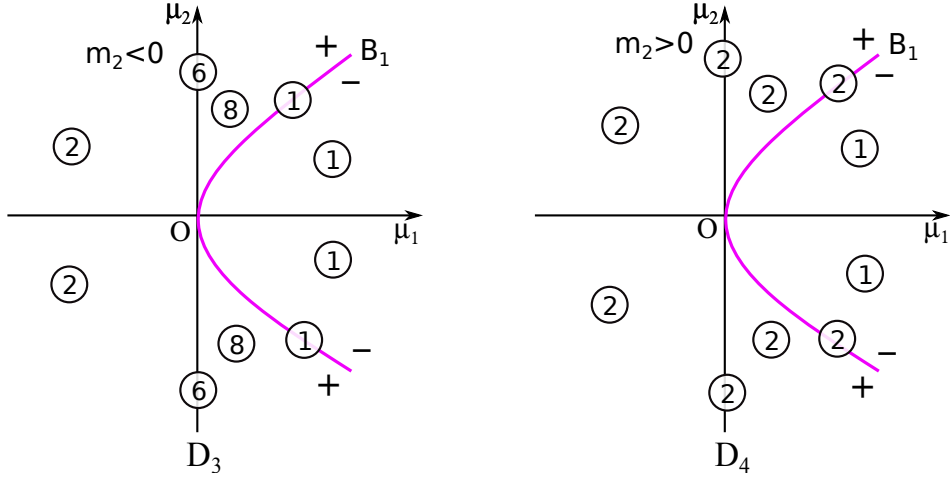
Figure 2: Bifurcation diagrams corresponding to $L_0 > 0$, $c_1 d_1 \neq 0$, respectively, $m_2 < 0$ and $m_2 > 0$.
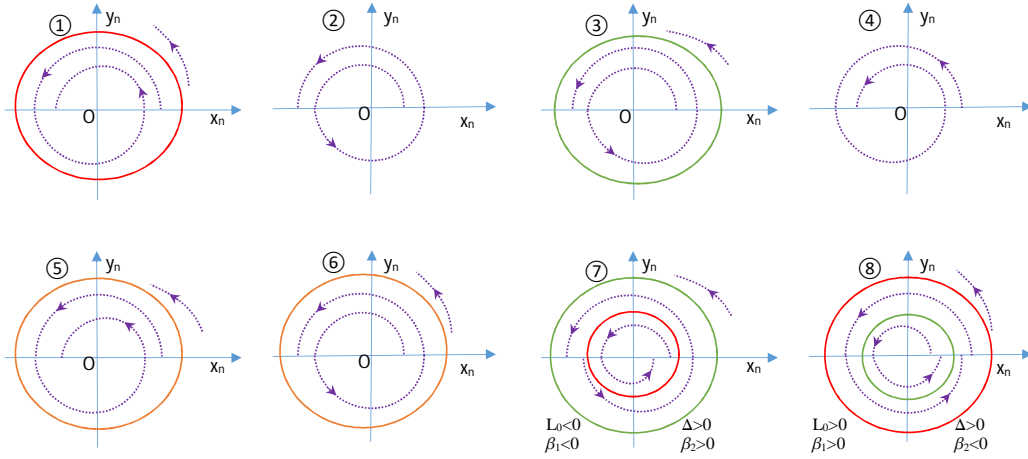

Figure 3: Generic phase portraits of the system (8)-(9).

the form

$$\alpha_1 = -\frac{3}{4}\mu_1 - \mu_2 + s_{20}\mu_1^2 + s_{11}\mu_1\mu_2 + s_{02}\mu_2^2 \qquad \text{and} \qquad \alpha_2 = \frac{1}{2}\mu_1 + \mu_2 + p_{20}\mu_1^2 + p_{11}\mu_1\mu_2 + p_{02}\mu_2^2.$$

Using the method of undetermined coefficients in (13), we obtain a linear system in the unknowns s_{ij} and p_{ij}, $i + j = 2$, whose solution is $p_{02} = 7$, $p_{11} = \frac{17}{2}$, $p_{20} = \frac{89}{32}$, $s_{02} = -10$, $s_{11} = -\frac{49}{4}$ and $s_{20} = -\frac{261}{64}$. These lead to $\widehat{L}_2(\mu) = 1 + \frac{1}{4}\mu_1 + \mu_2 + 5\mu_2^2$ and $\widehat{\beta}_2(\mu) = -\frac{1}{4}\mu_1 - 5\mu_2^2$ in their lowest terms, thus, $m_2 = -5$.

We notice that $m_2 = -5$ could be obtained directly from the coefficients of $\beta_{1,2}(\alpha)$ and $L_2(\alpha)$ by formula (23).

Using S^{-1} up to quadratic terms is not sufficient for finding $\widehat{\beta}_1(\mu)$. However, $\widehat{\beta}_1(\mu)$ can be determined from the substitution (13) by $\widehat{\beta}_2^2(\mu) - 4\widehat{\beta}_1(\mu)\widehat{L}_2(\mu) - \mu_1 = 0$, which yields $\widehat{\beta}_1(\mu) = -\frac{1}{4}\mu_1 + 25\mu_2^4$ in their lowest terms. Since $L_0 = 1$ and $m_2 = -5$, the corresponding bifurcation diagram of the map (27) is D_3, Figure 2.

Let us illustrate numerically the behavior of the map (27) for different values of $\alpha = (\alpha_1, \alpha_2)$ corresponding to the four different regions of D_3, which we denote by R_1, R_2, R_6 and R_8.

To this end, we proceed as it follows. For a given numerical value (α_1, α_2), we determine $\mu = (\mu_1, \mu_2)$ by the transformation S from $\mu_1 = \beta_2^2(\alpha) - 4\beta_1(\alpha)L_2(\alpha)$ and $\mu_2 = \beta_2(\alpha) + L_2(\alpha) - L_0$, and find the region of D_3 where μ lies. Thus, the behavior of the map (27) should be in agreement with the corresponding region. To probe this, we integrate numerically the map in Matlab, with (α_1, α_2) fixed in the begining, and find different orbits (x_n, y_n), where $x_n = \rho_n \cos \varphi_n$ and $y_n = \rho_n \sin \varphi_n$, for n taking all integer values from 1 to a fixed value N. The cartesian values x_n and y_n are then plotted in the same diagram.

Consider first $\alpha_1 = -0.017$ and $\alpha_2 = 0.015$, which lead to $\mu_1 = \Delta(\alpha) = 4.8579 \times 10^{-3}$ and $\mu_2 = 1.0782 \times 10^{-2}$, respectively, $\widehat{\beta}_1(\mu) = -1.2141 \times 10^{-3}$ and $\widehat{\beta}_2(\mu) = -1.7958 \times 10^{-3}$, thus, $(\mu_1, \mu_2) \in R_1 \in D_3$, with $\sqrt{y_1} = 0.18876$. For these values and $\theta_0 = 0.05$, three orbits are obtained and presented in Figure 4(a). The first orbit (magenta) starts at $(\rho_1, \varphi_1) = (0.17, 0)$ and tends to the origin $(0, 0)$ as n increases from 1 to $N = 800$. The second orbit (blue) approximates an invariant closed curve (which is a circle); it starts at $(\rho_1, \varphi_1) = (0.18876, 0)$ and was obtained with $N = 400$. The third orbit (red) starts at $(0.195, 0)$; it departs from the invariant closed curve for n increasing and may escape to infinity. It follows that, the closed invariant circle is unstable. We notice that, the three orbits from Figure 4(a) are in perfect agreement with the phase portrait 1 presented schematically in Figure 3.

For the second region R_2, let $\alpha_1 = -0.015$ and $\alpha_2 = 0.015$, which lead to $\mu_1 = \Delta(\alpha) = -2.7 \times 10^{-3}$ and $\mu_2 = 1.4778 \times 10^{-2}$, respectively, $\widehat{\beta}_1(\mu) = 6.8 \times 10^{-4}$ and $\widehat{\beta}_2(\mu) = -4 \times 10^{-4} < 0$, thus, $(\mu_1, \mu_2) \in R_2 \in D_3$. An orbit for these values and $\theta_0 = 0.03$, $N = 700$, $(\rho_1, \varphi_1) = (0.001, 0)$, is presented in Figure 4(b). The orbit departs from the origin and may escape to infinity, which is in agreement with the phase portrait 2 from Figure 3. We notice that R_2 may contain points (μ_1, μ_2) with $\widehat{\beta}_2(\mu) > 0$, which occurs, for example, at $\alpha_1 = 0.015$ and $\alpha_2 = 0.015$, which yield $\mu_1 = -0.127$ and $\mu_2 = 0.075$, respectively, $\widehat{\beta}_1(\mu) = 0.032$ and $\widehat{\beta}_2(\mu) = 0.0031$. The orbits simulated for these values are also in agreement with Figure 3.

In the third case, let $\alpha_1 = -0.015719$ and $\alpha_2 = 0.015$, which lead to $\mu_1 = \Delta(\alpha) = 0$ and $\mu_2 = 1.3341 \times 10^{-2}$, respectively, $\widehat{\beta}_1(\mu) = 6.1 \times 10^{-7}$, $\widehat{\beta}_2(\mu) = -8.9 \times 10^{-4}$ and $\sqrt{y_{1,2}} = 0.0242$, thus, $(\mu_1, \mu_2) \in R_6 \in D_3$. Setting $\theta_0 = 0.02$ and $N = 1000$, two orbits are depicted in Figure 4(c). One (blue) starts at $(\rho_1, \varphi_1) = (0.024223, 0)$ and approximates a closed invariant orbit (circle), while the other (magenta) starts at $(0.1, 0)$ and departs from the closed invariant orbit. Orbits starting from the interior of the invariant circle tend slowly to the circle for n increasing. Thus, the invariant circle is stable from the interior and unstable from the exterior. This behavior is in agreement to the phase portrait 6 from Figure 3.

Finally, let $\alpha_1 = -0.5$ and $\alpha_2 = 0.05$. Then $\Delta(\alpha) > 0$, $\rho_1 = \sqrt{y_1} = 0.6718$ and $\rho_2 = \sqrt{y_2} = 0.3699$, which, by S, lead to $\mu_1 = \Delta(\alpha) = 0.0714$ and $\mu_2 = -0.6498$, respectively, $\widehat{\beta}_1(\mu) = 4.4$ and $\widehat{\beta}_2(\mu) = -2.1$, that is, $(\mu_1, \mu_2) \in R_8$ from D_3. Numerical simulations of this case with $\theta_0 = 0.03$ are presented in Figure 4(d). Notice the appearance of two invariant closed curves, one stable (blue) and the other (red) unstable. This is in perfect agreement with the phase portrait 8, presented schematically in
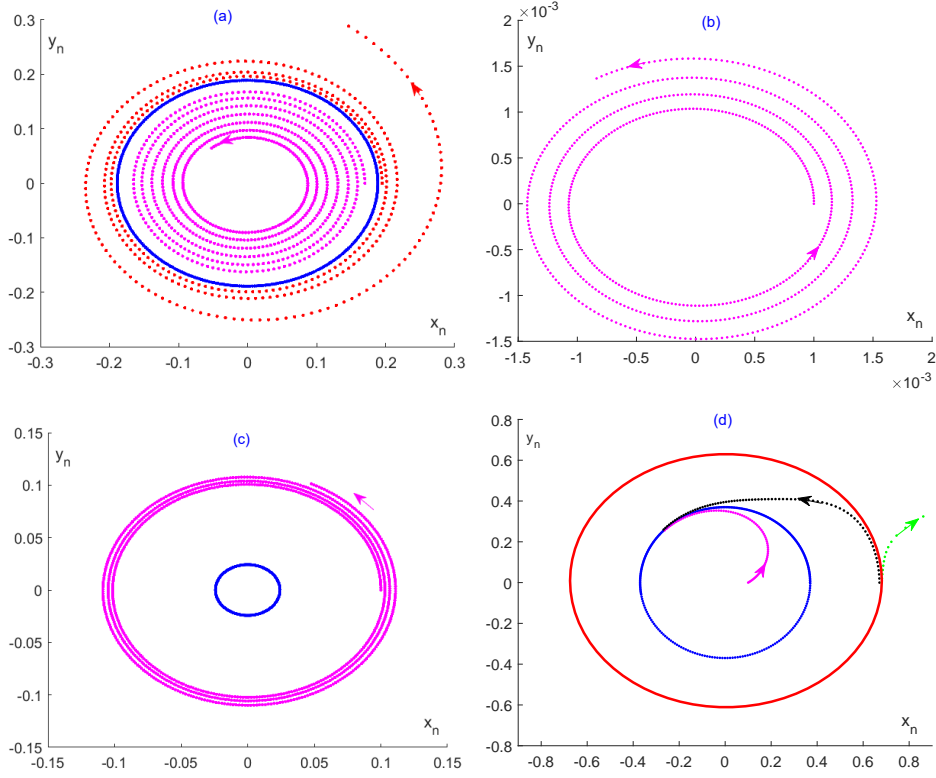
Figure 3.

Figure 4: The behavior of the map (27) on the four regions of the bifurcation diagram D_3.

5 Conclusions

The study we performed in this work brings to light new generic properties of a degenerate form of the Chenciner bifurcation. The degeneracy we tackled refers at the regularity of the transformation of parameters, which is used for obtaining a normal form in nondegenerate case. We studied the bifurcation when the transformation of parameters is not regular at $(0,0)$, thus, the classical results can not be applied. We proposed a different change of parameters, which was proved to be successful for approaching the degeneracy. More exactly, when the degeneracy condition occurs, the new transformation is regular at $(0,0)$ and, more importantly, can be used for studying the bifurcation. The cost of using this transformation is the appearance of a different generic condition. The new condition uses different coefficients to exist than the classical one, thus, they are complementary one to another. We exemplified the application of the method developed in this work on a particular map, which cannot be studied with the method used for nondegenerate case. When the both generic conditions fail, a new study is needed for exploring the behavior of the Chenciner bifurcation. This remains an open problem.

11

6 Acknowledgments

References

[1] Bakri, T., Kuznetsov, Y. A., & Verhulst, F. [2009] "Torus bifurcations in a mechanical system", *Journal of Dynamics and Differential Equations* **27**, 371-403.

[2] Broer, H. W., Holtman, S. J., Vegter, G. & Vitolo, R. [2009] "Geometry and dynamics of mildly degenerate Hopf–Neimarck–Sacker families near resonance", *Nonlinearity* **22**, 2161–2200.

[3] Chenciner, A. [1985] "Bifurcations de points fixes elliptiques. II. Orbites periodiques et ensembles de Cantor invariants", *Invent. Math.* **80**, 81–106.

[4] Chenciner, A. [1988] "Bifurcations de points fixes elliptiques. III. Orbites periodiques de petites periodes," *Inst. Hautes Etudes Sci. Publ. Math.* **66**, 5-91.

[5] Chenciner, A., Gasull, A. & Llibre, J. [1987] "Une description complete du portrait de phase d'un modele d'elimination resonante", *C. R. Acad. Sci. Paris Ser. I Math.* **305 (13)**, 623–626.

[6] Dettmann, C.P. , Fain, V. & Turaev, D. [2018] "Splitting of separatrices, scattering maps, and energy growth for a billiard inside a time-dependent symmetric domain close to an ellipse", *Nonlinearity* **31 (3)**, 667–700.

[7] Floudas, C. A. & Lin, X. "Continuous-time versus discrete-time approaches for scheduling of chemical processes: a review", *Computers and Chemical Engineering* **28**, 2109–2129.

[8] Gelfreich, V. & Turaev, D. [2017] "Arnold diffusion in a priori chaotic symplectic maps", *Communications in Mathematical Physics* **353(2)**, 507–547.

[Guirao & Llibre, 2019] Guirao, J.L.G. & Llibre, J. [2019] "On the periods of a continuous self-map on a graph", *Computational and Applied Mathematics*, **38(2)**, 1–79.

[9] Jangveladze, T., Kiguradze, Z. & Gagoshidze, M. [2019] "Economical Difference Scheme for One Multi-Dimensional Nonlinear System", *Acta Mathematica Scientia* **39**, 971–988.

[10] Khanin, K. & Kocic, S. [2019] "Hausdorff dimension of invariant measure of circle diffeomorphisms with a break point", *Ergodic Theory and Dynamical Systems* **39(5)**, 1331–1339.

[11] Kuznetsov, Y.A. [2004] *Elements of Applied Bifurcation Theory*, 3rd Ed. (Springer–Verlag, 2004).

[12] Llibre, J. & Sirvent, V. F. [2018] "On Lefschetz periodic point free self-maps", *Journal of Fixed Point Theory and Applications* **20(1)**, 1–38.

[13] Pesin, Y., Senti, S. & Zhang, K. [2019] "Thermodynamics of the Katok map", *Ergodic Theory and Dynamical Systems* **39(3)**, 764–794.

[14] Tigan, G. & Constantinescu, D. [2016] "Bifurcations in a family of Hamiltonian systems and associated nontwist cubic maps", *Chaos, Solitons and Fractals* **91**, 128–135.

[15] Tigan, G., Lugojan, S. & Ciurdariu, L. [2020] "Analysis of Degenerate Chenciner Bifurcation", *International Journal of Bifurcation and Chaos*, **30(16)**, 1–11.

[16] Vitolo, R., Broer H. & Simo, C' [2010] "Routes to chaos in the Hopf-saddle-node bifurcation for fixed points of 3D-diffeomorphisms", *Nonlinearity* **23**, 1919–1947.

[17] Wiggins, S. [2003] *Introduction to applied nonlinear dynamical systems and chaos, Vol. 2*, Springer Science & Business Media, 2003.